Enhancing Poly (lactic acid) Microcellular Foams by Formation of Distinctive Crystalline Structure

[1]Ruiguang Li, [1]Lin Ye, [1]Xiaowen Zhao*, [2]Phil Coates, [2]Fin Caton-Rose

1. State Key Laboratory of Polymer Materials Engineering of China, Polymer Research Institute of Sichuan University, Chengdu, China

2. School of Engineering, Design and Technology, University of Bradford, Bradford, U.K.

*: Corresponding author: Xiaowen Zhao

Address: State Key Laboratory of Polymer Materials Engineering

Polymer Research Institute of Sichuan University, Chengdu 610065, China

E-mail: zhaoxiaowenscu@126.com

Tel: 86-28-85408802

Fax: 86-28-85402465

Enhancing Poly (lactic acid) Microcellular Foams by Formation of Distinctive Crystalline Structure

[1]Ruiguang Li, [1]Lin Ye, [1]Xiaowen Zhao*, [2]Phil Coates, [2]Fin Caton-Rose

1. State Key Laboratory of Polymer Materials Engineering of China, Polymer Research Institute of Sichuan University, Chengdu, China

2. School of Engineering, Design and Technology, University of Bradford, Bradford, U.K.

Abstract: By controlling the crystallization behavior of Poly (lactic acid) (PLA) in presence of hydrazide nucleating agent (HNA), PLA-HNA foams with enhanced microcellular structure were prepared via supercritical CO_2 foaming. It was found that HNA can self-assemble into fibrillar networks, inducing the crystallization of PLA on their surface, and "shish-kebab" crystalline structure with high crystallinity formed, which can be maintained during the whole foaming process. Incorporation of HNA promoted the formation of gt conformers, improved the amount of dissolved CO_2, hindered the escape of CO_2, and increased the viscoelasticity of PLA. Compared with neat PLA foam, for PLA-HNA foam, the average cell diameter decreased obviously, from 64.39 to 6.59μm, while the cell density increased up to nearly three orders of magnitudes, from 6.82×10^6 to 4.44×10^9 cells/cm^3. Moreover, lots of fibrillar structure appeared and entangled with each other on the cell wall of the foam. By forming such dense micropores and enhanced fibrillar structures, PLA foam was highly reinforced with significantly improved compressive strength.

Keywords: Poly (lactic acid) (PLA); Microcellular foam; Enhanced crystalline structure; Foaming behavior; Reinforcing mechanism

1. Introduction

Microcellular foams, which are usually characterized by a cell size less than 10 μm and a cell density greater than 10^9 cells/cm^3, exhibit significant advantages over

ordinary foams, such as high impact toughness, superior heat and sound insulation properties.[1-8] At present, the preferential way to prepare microcellular foam is supercritical CO_2 ($scCO_2$) foaming, which applies non-toxic, nonflammable and inexpensive CO_2 as the blow agent.[9, 10] Although some microcellular foams have been prepared via supercritical CO_2 foaming in recent decades, from amorphous to semi-crystalline polymers, such as PP, PS, and so on,[11-13] the overuse of such petroleum-based polymers not only consumes lots of petrochemical energy, but also brings about series of ecological environment problems.

Poly (lactic acid) (PLA), a biobased and biodegradable aliphatic polyester, derived from renewable resources such as corn and sugarcane, has been considered as the most promising replacement for petroleum-based polymer due to its outstanding mechanical properties and good processing ability.[14-17] However, PLA usually exhibits low viscoelasticity at processing temperature as a consequence of its linear structure and slow crystallization kinetics, which could negatively affect cell growth and cell uniformity during foaming process due to cell coalescence and cell-wall rupture. And thus the preparation of microcellular PLA foams with uniform cell morphology remains challenging.

At present, some methods have been proposed to improve the foaming behavior of PLA, such as chain extension, chain branching, and blending with other materials.[18-23] Moreover, controlling crystallization kinetics of PLA during foaming has also been recognized as an effective way to improve its foaming behavior. Li *et al.* reported a new supercritical fluid foaming process based on pre-isothermal cold crystallization for PLA, and foams with high expansion ratio were obtained.[24] Tiwary *et al.* prepared chain branched PLA containing nucleating agent through reactive extrusion, and very fine, sub-micron sized foams were obtained.[25] Nieddu *et al.*

studied the foaming behavior of PLA/nanoclay composites by using CO_2 as blowing agent. It was found that, both cell nucleation and growth behaviors of PLA were improved due to the more rapid crystallization kinetics triggered by the presence of nanoclay.[26] Wang *et al.* incorporated chain extender (CE) as well as hydroxyl-functionalized graphene (HG) into PLA to improve the crystallization behaviors and rheological properties of PLA, and foams with nanocellular structure were obtained.[27] Based on PLA/graphene oxide (GO) nanocomposites, Geng *et al.* also prepared composite foams with nanopores via supercritical CO_2 foaming at low temperature.[28] In conclusion, at present, for the purpose of foaming, the improvement in crystallinity of PLA has been usually achieved by pre-isothermal/pre-non-isothermal crystallization treatment or incorporation of nano-particles as heterogeneous nucleators in PLA, such as nanosilica, nanoclay and graphene, and so on.[29]

Self-assembling nucleating agents can be dissolved in polymer melt and then self-assemble into special frameworks upon cooling, such as needle-like, dendritic and flower-like crystals, inducing the crystallization of polymer with sorts of crystalline morphology.[30] Hydrazide nucleating agent (HNA) with structural feature of containing a large number of functional polar groups like C=O and N-H, can also recrystallize and self-assemble into fibrillar or dendritic crystalline structure upon cooling due to the association of hydrogen bonds between HNA molecules. In this work, by controlling the crystallization behavior of PLA in presence of HNA, the enhanced fibrillar crystalline structure with high crystallinity was expected to form for PLA, which was very beneficial for enhancing the viscoelasticity and improving the foaming ability of PLA matrix, and thus PLA-HNA foams with microcellular structure could be prepared. The formation of the enhanced crystalline structure for

PLA-HNA was studied, while the influence of HNA content on the foaming behavior, microcellular structure and mechanical properties of PLA foam was discussed. Furthermore, the formation mechanism of the enhanced microcellular structure for PLA-HNA foams was explored.

2. Experimental

2.1 Materials

Poly (L-lactic acid) (PLA) comprising 2% DLA (NatureWorks® 3052D) was provided by Nature Works Co., USA. The molecular weight (M_w) and the polydispersity was about 1×10^5 and 1.21, respectively, and the melt flow index was 14 g/10min. The glass transition temperature of PLA (T_g) was about 58^{o}C and the melting temperature (T_m) was about 156^{o}C. Hydrazide nucleating agent (HNA) with analytical grade was supplied by Shanxi Provincial Institute of Chemical Industry, China. The molecular weight (M_w) of HNA was 438 and the density was about 1.16 g/cm^3. The chemical structure of HNA was shown in Figure 1.

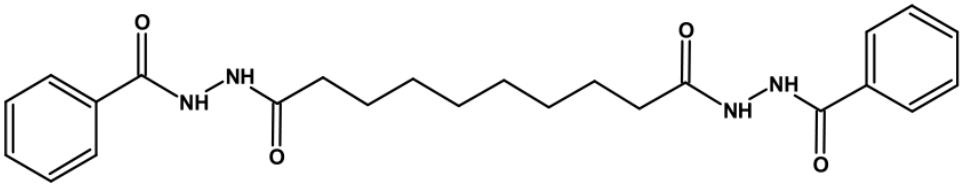

Figure 1. Chemical structure of HNA

2.2 Preparation of PLA microcellular foam

A HAAKE internal mixer (Thermo Scientific, U.S.A.) was used to prepare PLA samples containing various amounts of HNA. After compounding by the mixer for 10min, the product was compression molded into sheets at 200^{o}C and 10MPa for 5min, followed by cooling to 30^{o}C (the cooling rate was 2^{o}C/min). Then the sheets were cut into squares with dimensions of 10×10 mm^2 for foaming.

The PLA microcellular foams were prepared by batch foaming process by using

sc-CO_2 as foaming agents. The sample was put into a self-made high-pressure vessel with volume of 1L and then was pre-heated to 150^{o}C. The pressure of the vessel was controlled by a supercritical fluid pump (TELEDYNE ISCO 500D, Lincoln, Nebraska) with control precision of 0.01MPa. The temperature control precision of the vessel was about 1^{o}C. Then, after flushed by low pressure CO_2 for 5 min, the vessel was pressurized to 18MPa. After saturation for 2h, the sample underwent a rapid quench of pressure (the decompression rate was about 4MPa/s) for cell nucleation and growth. Finally, after the vessel was cooled down with a water cooling system, the sample was removed from the vessel and foam product was obtained.

2.3 Measurements

2.3.1 Polarized optical microscopy (POM) analysis

The crystalline morphology of PLA samples was observed by an Olympus BX51 microscopy (Olympus Co., Japan) equipped with a HCS 302 hot-stage (INSTEC, USA). Before observation, slice sample with thickness of 20μm was prepared.

2.3.2 In-situ FTIR analysis

The time-dependent IR absorbance spectrum of PLA samples were recorded by using a Nicolet-IS10 (Thermo Electron Co., USA) spectrometer with a 4 cm^{-1} spectral resolution. The measurement was conducted under the protection of nitrogen and the baseline correcting process was performed by using the automatic baseline correction of OMNIC 8.2 spectral collecting software (Thermo Fisher Scientific Inc., USA).

2.3.3 Differential scanning calorimetry (DSC) analysis

The non-isothermal crystallization analysis of PLA samples was performed with a Netzsch 204 differential scanning calorimetry (DSC) (Phoenix Co, Germany). X_c can be obtained with the following formula:

$$X_c=[(\Delta H_m-\Delta H_c)/\Delta H_0]*100\% \qquad (1)$$

where ΔH_m and ΔH_c were the melting enthalpies and cold crystallization enthalpies for the samples; ΔH_0 was the melting enthalpy of 100% crystalline PLA which was 93J/g.[31]

2.3.4 The amount of dissolved CO_2

A gravimetric method was applied to determine the amount of CO_2 dissolved in PLA samples.[28] The original weight of PLA samples was measured by an electronic balance readable to 0.0001 g, and then samples were placed into the high-pressure vessel under a CO_2 gas pressure of 18MPa at 150^oC (the same as the foaming condition) for a certain time to absorb CO_2. Afterward, the vessel was slowly depressurized with a pressure relief rate of 0.5MPa/s (to avoid foaming), and the CO_2-absorbed samples were taken out and weighed immediately. The results showed in this work were an average of the data for five samples.

The amount of CO_2 dissolved in PLA samples can be determined with the following formula:

$$\text{The amount of dissolved } CO_2=(W_t-W_i)/W_i \quad (2)$$

where M_i and M_t were the masses of the sample before and after absorption, respectively.

Furthermore, the weight loss of the saturated PLA samples during desorption process over time at atmosphere pressure was measured. After saturated for 2h at 18MPa and 150^oC, samples were removed from the vessel immediately and weighed at regular time intervals. The weight loss of PLA samples can be calculated as follows:

$$\text{Weight loss}= [(W_i-W_t)/W_i]*100\% \quad (3)$$

where M_i was the mass of saturated sample and M_t was the mass of the sample after desorption. The results showed in this work were an average of the data for five samples.

2.3.5 Scanning electron microscope analysis (SEM)

The analysis of the crystalline structure and cellular structure for PLA samples was performed with a JEOL JSM-5900LV scanning electron microscope (JEOL co, Japan).[32] The average cell diameter as well as the cell density of the PLA foams was estimated by using image analysis software (Image Pro Plus, USA). The cell density was calculated with Eq. (4):

$$N_f = (nM^2/A)^{3/2} \quad (4)$$

where N_f was cell density of the sample; n was the number of cells in specific region; M was the magnification factor and A was the area of specific region.

2.3.6 Dynamic mechanical analysis

Dynamic mechanical analysis (DMA) of PLA samples was performed with a Q800 DMA instruments (TA Instruments, USA) according to ISO 6721-1-2019. Samples were measured with a stretching mode under a frequency of 1 Hz. The temperature range was 30~200^{o}C and the heating rate was 3 ℃/min. The dynamic load of 5N and amplitude of 15% were applied. The dimension of the sample was 25×5×1 mm^3. The results showed in the work were an average of the data for five samples.

2.3.7 Mechanical properties

The compressive properties of PLA foams were measured by the 4302 material testing machine (Instron Co., USA) at room temperature according to ISO 844-2004. The foam was compressed to 50% of the initial thickness at room temperature. The dimension of the sample was 10×10×4 mm^3 and the test speed was 5 mm/min. The results showed in the work were an average of the data for five samples.

3. Results and Discussion

3.1 Formation of Enhanced Distinctive Crystalline Structure of PLA-HNA

The preparation process of PLA-HNA microcellular foams included two steps: compression molding process and batch foaming process. In the compression molding process, PLA-HNA samples were compression-molded at 200℃ and cooled with a cooling rate of 2^{o}C/min to promote the formation of perfect crystalline structure in the sample. In the batch foaming process, samples were saturated with CO_2 for 2h at 150^{o}C and 18MPa, followed by a rapid release of pressure for cell nucleation and growth, and quenched to room temperature. The influence of HNA on the crystalline structure of PLA at different stage of foam-preparation process was studied.

As shown in Figure 2, for neat PLA, during the first cooling process from 200^{o}C to 30^{o}C, a small amount of spherulites began to precipitate at 116^{o}C, while the spherulite growth was basically completed at 90^{o}C, and only sparse spherulites were observed at 30^{o}C. For PLA-0.5wt% HNA, no precipitate can be observed at 200^{o}C, and when the temperature dropped to 118^{o}C, unique macroscopic short fibrillar structure attributed to the self-organization of HNA molecules can be observed. When the temperature further dropped to 114^{o}C, it was interesting to find that not only more HNA fibrils formed but also PLA crystals grew perpendicularly to the long axis of the fibrils, forming a unique shish-kebab-like structure. For PLA-2wt% HNA, some fibrillar structure can be found in PLA melts at 200^{o}C, indicating that HNA was not completely dissolved in PLA melt. When the temperature dropped to 140^{o}C, more and more HNA fibrils precipitated, forming a hybrid dendritic network structure, while PLA began to crystallize on the surface of HNA at 130^{o}C. Compared with PLA-0.5wt% HNA, for PLA-2wt% HNA, the aspect ratio of fibrils became larger and the packing density of the fibrils was much higher, forming a large amount of shish-kebab

structure. When the samples were re-heated to 150°C for sorption of CO_2 and then quenched to room temperature, most of the crystalline structure was maintained for all samples, as shown in Figure 2.

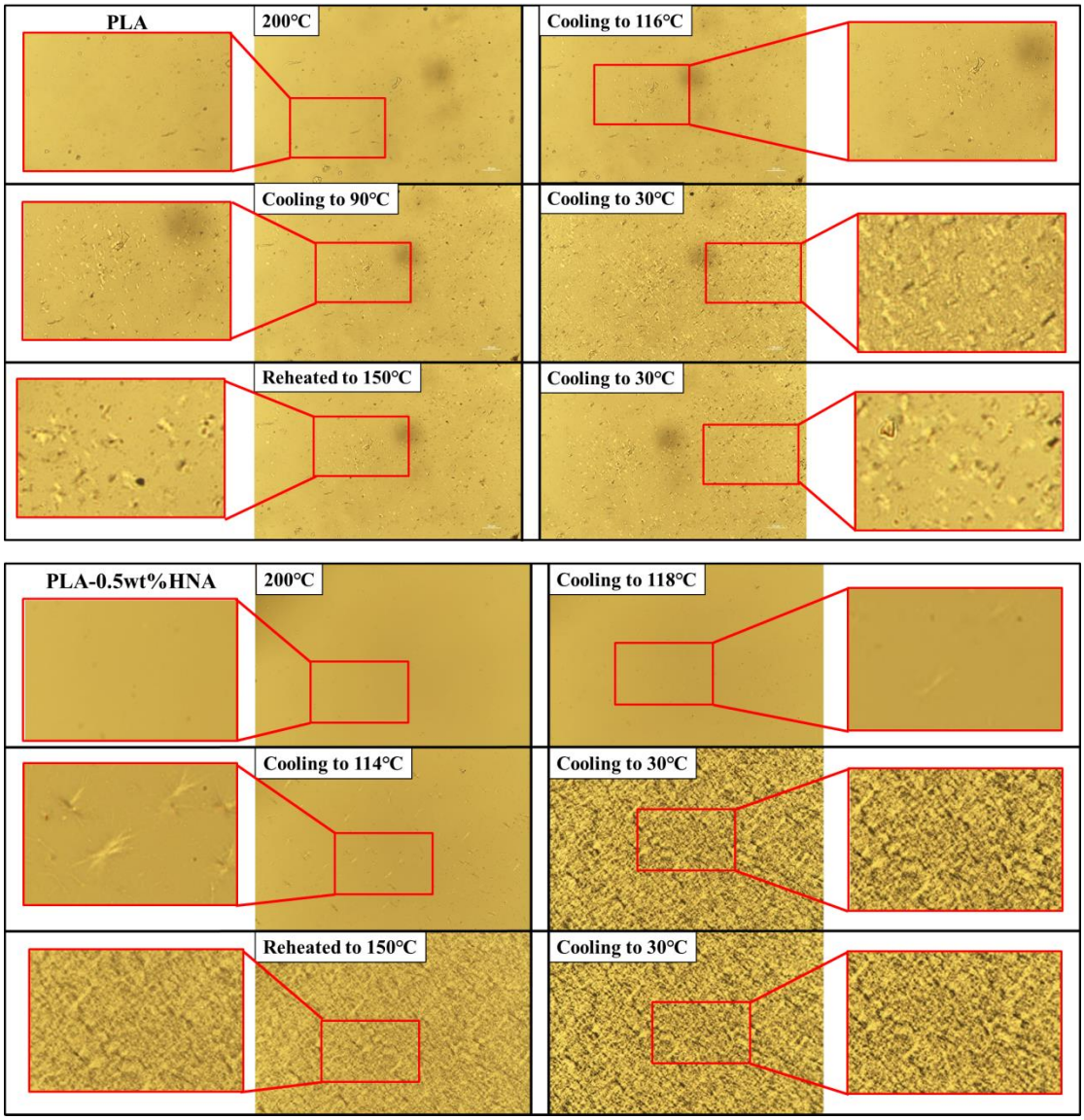

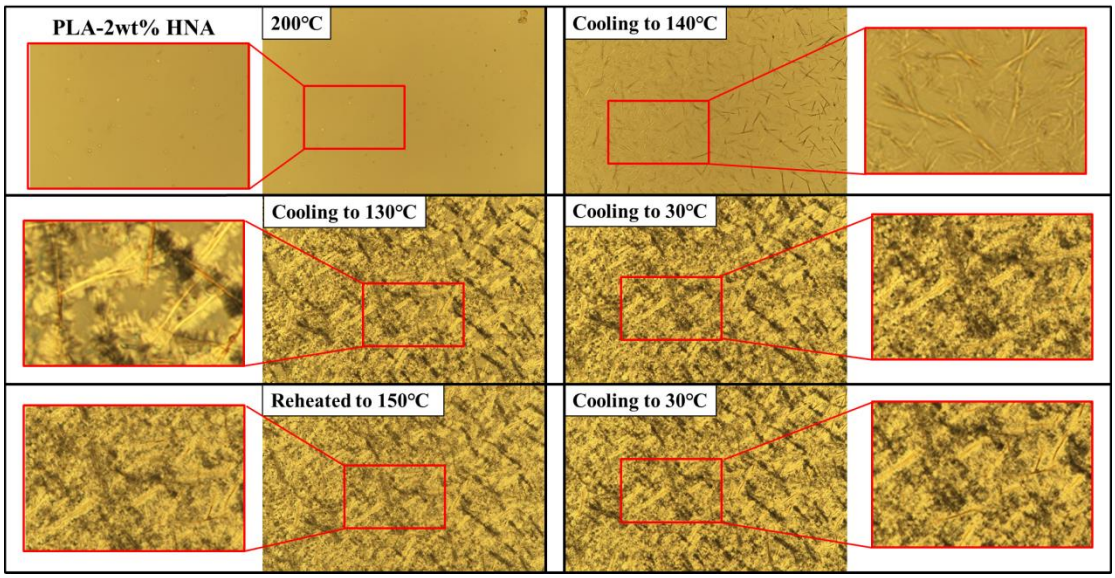

Figure 2. POM images of PLA, PLA-0.5wt% HNA and PLA-2wt% HNA corresponding to the thermal history during the mold-pressing process and foaming process

More microscopic information about the crystalline structures of PLA samples with and without HNA at 30^{o}C was obtained by SEM analysis. Before observation, samples were etched with a methanol-water mixture solution (1:2 by volume) containing 0.025 mol/L sodium hydroxide to selectively remove both the HNA frameworks and the amorphous regions from PLA crystals. As shown in Figure 3, for neat PLA, lots of holes can be observed on the surface of the sample, which was attributed to the etched amorphous phase. For the samples with 0.5wt% HNA, it can be seen that HNA self-assembled into fibrils with random arrangement in PLA matrix (the red bars depicted in SEM images represented the HNA fibrils which were etched away by the solution), and the “shish-kebab” structure can be observed. The “kebab” was originated from the overlap of PLA lamellae while the “shish” was originated from the HNA fibrils. With further increasing of HNA content, “shish-kebab” structures with more quantity and larger size can be found in the PLA matrix, which was consistent with the phenomenon observed by POM.

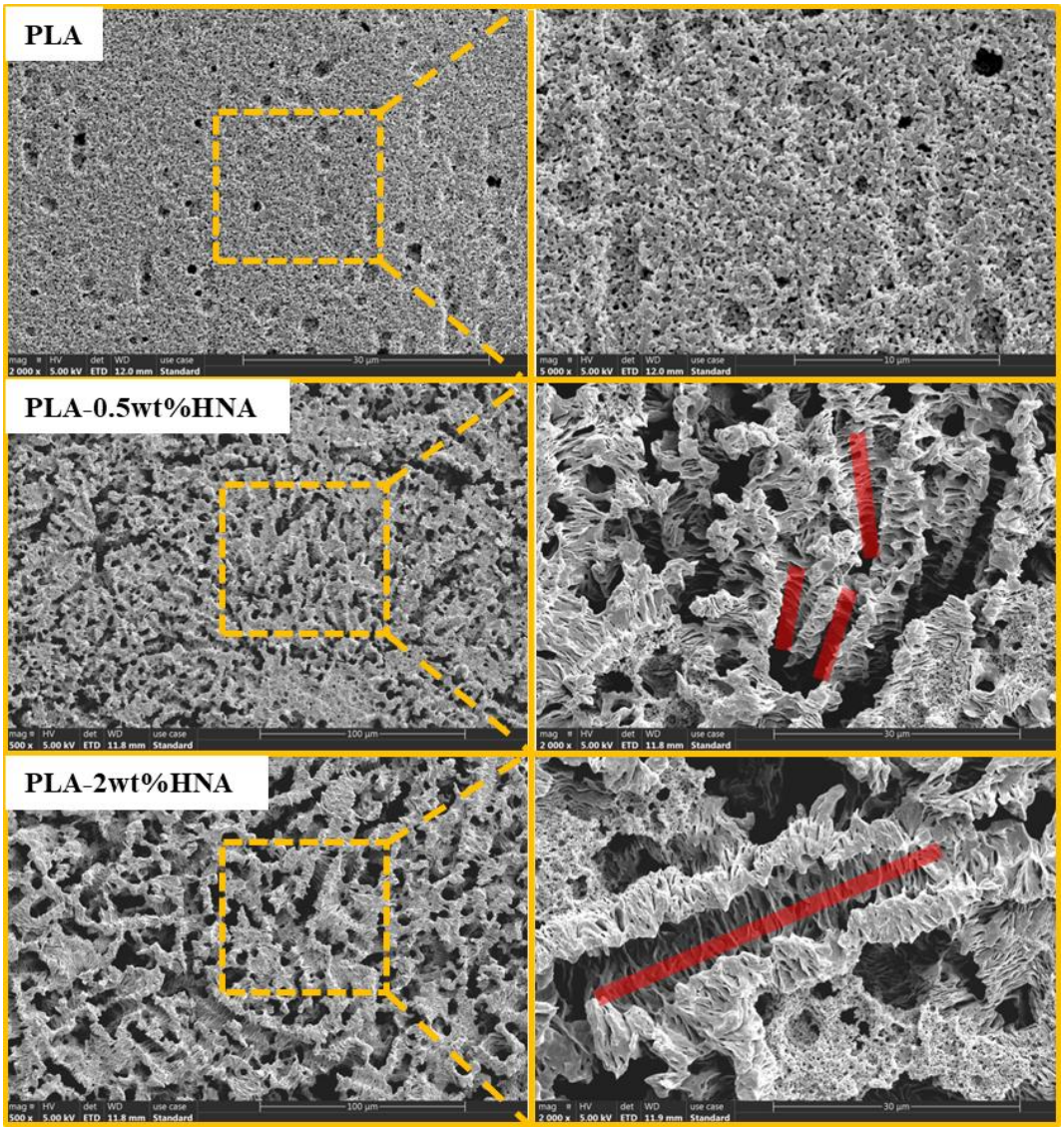

Figure 3. SEM micrographs of etched PLA, PLA-0.5wt% HNA and PLA-2wt% HNA

FTIR was used for studying the crystallization behavior of PLA-HNA samples.[33] Based on the rotational isomeric state (RIS) model, the infrared absorption peaks in the carbonyl region of PLA can be divided into four different conformational peaks: tt(1777 cm^{-1}), tg(1769 cm^{-1}), gt(1758 cm^{-1}), and gg(1747 cm^{-1}), respectively, as shown in Figure 4A. Among them, the gt conformer with the lowest energy formed 10_3 helix, which constituted the most stable α-crystal of PLA.

Figure 4(B, b) displayed the original spectra in the carbonyl stretching region of neat PLA and PLA-2wt% HNA recorded during the non-isothermal crystallization from 200^{o}C to 30^{o}C. With the decrease of temperature, the peak of the carbonyl

region of the both samples narrowed, while the maximum peak intensity increased. The difference spectra were obtained by subtracting the initial spectrum from the consecutive spectra, as shown in Figure 4(C, c). For both neat PLA and PLA-2wt% HNA, upon cooling, the intensity of gt conformer at 1758 cm^{-1} was positive, while intensities of other three peaks were negative, indicating that tt, tg and gg conformers transformed into gt conformer during crystallization. Meanwhile, compared with neat PLA, for PLA-2wt% HNA sample, when the temperature decreased, the variation of the peak intensity at 1758 cm^{-1} was greater, while the peak intensity at 1777 and 1747 cm^{-1} changed little, indicating that more gt conformer formed for PLA during crystallization by incorporation of HNA and thus lower energy barrier was required for the following formation of PLA α-crystal.

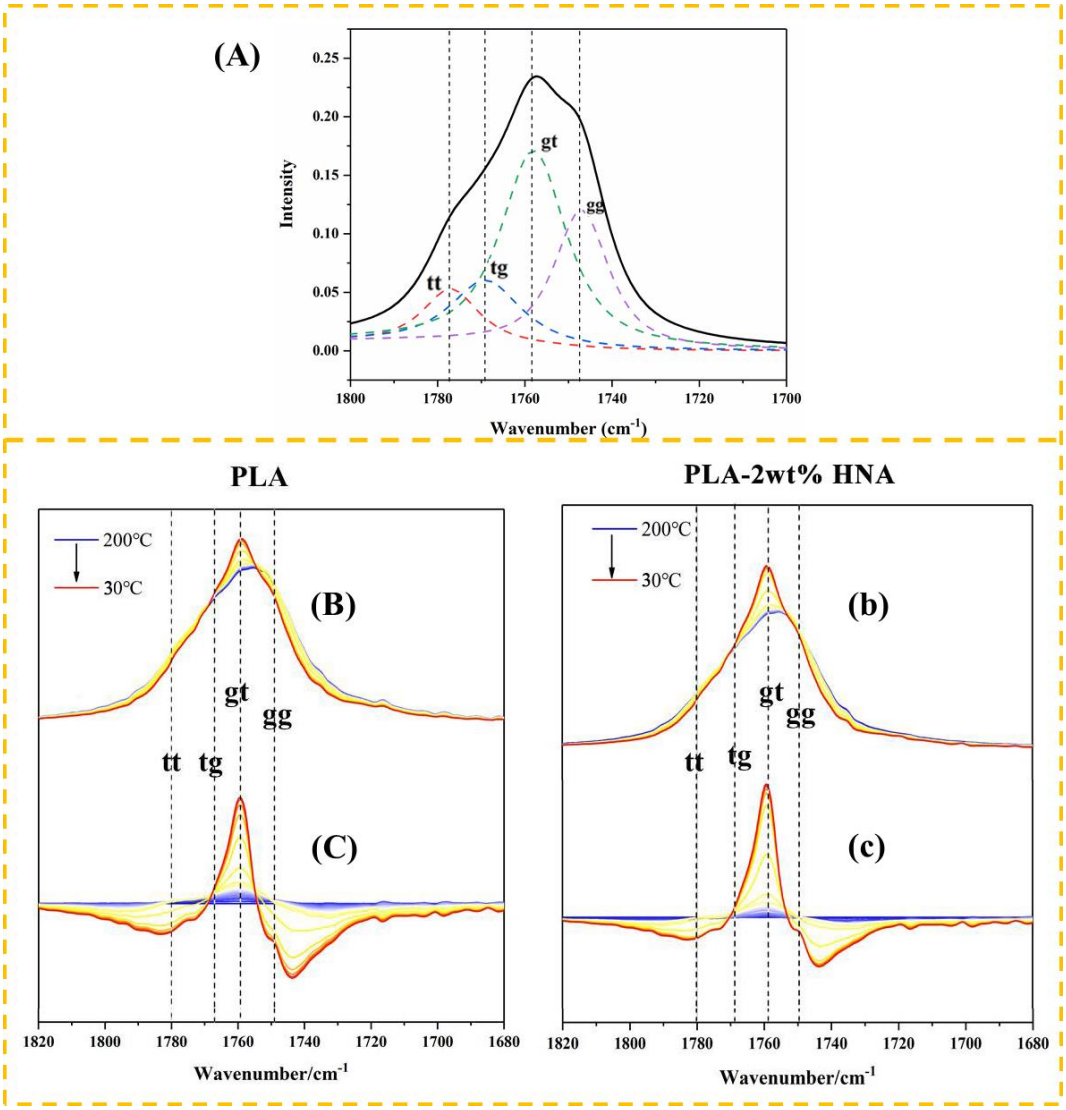

Figure 4. Peak distribution spectra for the carbonyl stretching region of PLA (A); time-resolved spectra of PLA (B) and PLA-2wt% HNA (b); the corresponding difference spectra of PLA (C) and PLA-2wt% (c)

Figure 5 presented the DSC curves of neat PLA and PLA-HNA with different HNA content at a heating rate of 10°C/min, from which the enthalpy of melting ($\triangle H$) and crystallinity (X_c) can be obtained, as listed in Tab.1. All samples exhibited three distinct peaks corresponding to glass transition at 60 ℃, cold crystallization peaks at about 90-120 ℃, and melting peaks at around 155 ℃ respectively. Neat PLA showed slow crystallization during cooling from the melt, and thus imperfect crystalline structure formed during the sample preparation process. In this case, obvious cold crystallization occurred during the heating process of DSC measurement. With the

increase of HNA content, the cold crystallization peak became smaller and moved to lower temperature. By introduction of HNA, the crystallization ability of PLA was enhanced greatly, and the crystallization can be almost completed during the sample preparation process, and thus the cold crystallization was weakened. Moreover, it was reported that PLA crystals showed a large tendency to reorganize into more stable structures through continuous partial melting–recrystallization–perfection mechanism during heating, resulting in a multiple melting behavior.[34] The melting peak at higher temperature was attributed to the melting of a more perfect crystalline structure formed by reorganization of PLA and the shoulder peak at lower temperature was contributed to the less perfect crystalline structure. By the introduction of HNA, the shoulder melting peak at lower temperature became smaller and even disappeared, indicating the formation of more perfect crystalline structures with high regular arrangement. Besides, as shown in Table 1, the melting enthalpy and crystallinity of PLA increased obviously with increasing HNA content, from 2.49% to 31.38%, suggesting that the crystallization of PLA can be promoted greatly by incorporation of HNA.

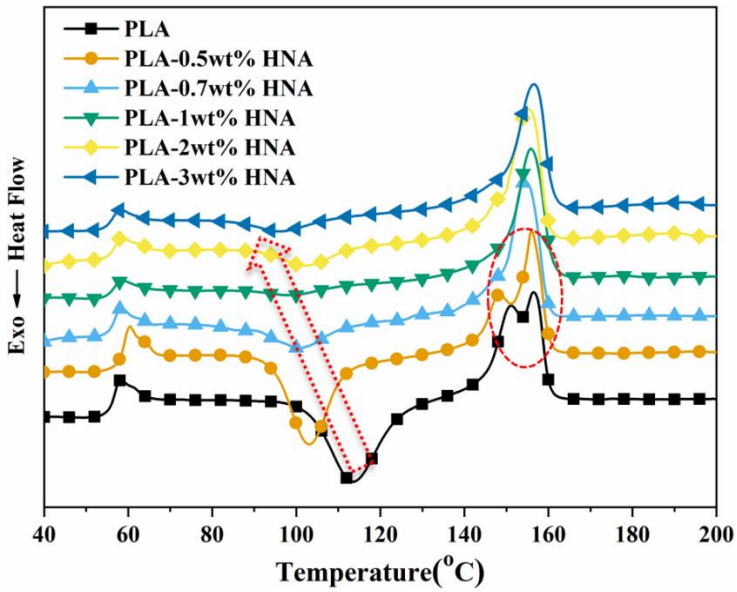

Figure 5. DSC curves of PLA-HNA with different HNA content

Table 1. DSC parameters of PLA-HNA with different HNA content

Sample	T_g(℃)	T_{m1}(℃)	T_{m2}(℃)	ΔH(J/g)	X_c(%)
PLA	56.2	152.3	156.5	2.32	2.49
PLA-0.5wt% HNA	57.2	149.2	156.4	5.48	5.89
PLA-0.7wt% HNA	56.4	-	154.6	23.24	24.98
PLA-1wt% HNA	56.6	-	155.8	27.17	29.22
PLA-2wt% HNA	56.8	-	155.4	28.67	30.83
PLA-3wt% HNA	56.9	-	156.6	29.18	31.38

The viscoelastic properties under foaming conditions were important for foaming behavior of materials. The DMA curves of PLA-HNA samples with different HNA content at foaming temperature was presented in Figure 6. By introduction of HNA, both storage modulus and loss modulus of PLA samples increased sharply, and compared with neat PLA, the storage modulus and loss modulus of PLA-3wt% HNA increased by 781% and 271%, respectively, indicating the significant enhancement of the viscoelasticity at the foaming temperature. Due to the retention of shish-kebab-like crystalline structure in PLA-HNA samples under foaming temperature, the stiffness of the material was improved, which was beneficial for PLA to resist excessive deformation under the stress.

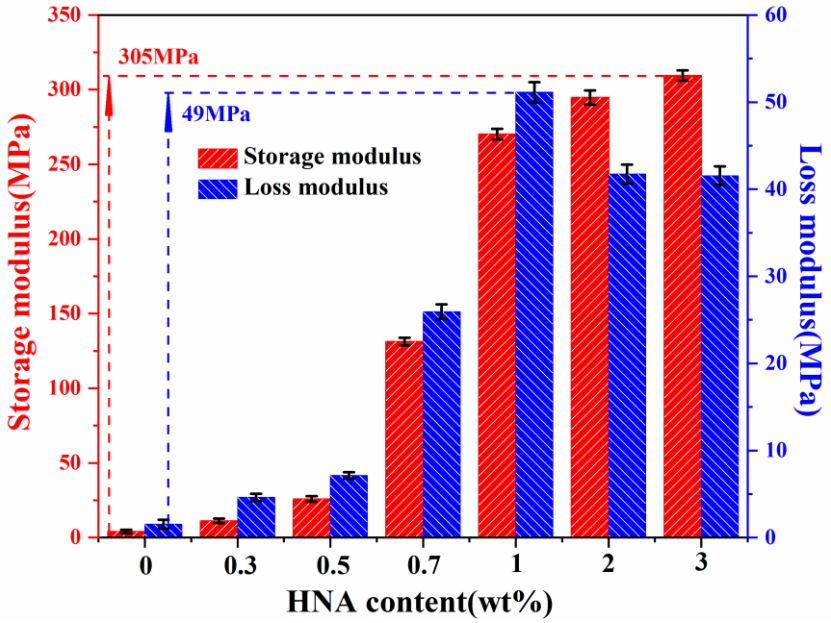

Figure 6. Storage modulus and loss modulus of PLA and PLA-HNA with different HNA content at foaming temperature

3.2 Foaming Behavior of PLA-HNA

Figure 7a showed the amount of CO_2 dissolved in neat PLA and PLA-HNA samples as a function of absorption time. It can be seen that, in the initial stage of adsorption, the amount of dissolved CO_2 for all samples increased rapidly with the increase of adsorption time, and then gradually stabilized, indicating that samples were fully saturated by CO_2. Furthermore, with the increase of HNA content, the saturated amount of CO_2 dissolved in the matrix increased at first and then declined slightly. Based on the result of DSC analysis, by incorporation of HNA, the crystallinity of PLA increased obviously, and thus a large amount of crystalline-amorphous interface formed. Such interface provided sorption sites for CO_2 and then the amount of CO_2 dissolved in PLA-HNA samples increased. However, because CO_2 can only be dissolved in the amorphous region, the amount of CO_2 dissolved in PLA decreased for PLA-3wt%HNA samples with high crystallinity. The desorption curves of CO_2 for the saturated samples were shown in Figure 7b. It can be seen that, the weight loss, i.e. CO_2 desorption ratio, of neat PLA and PLA-HNA increased at first and then reached equilibrium. Under the same desorption time, the

weight loss of samples decreased obviously with the increase of HNA content, indicating that less CO_2 overflowed from the sample. The phenomenon was attributed to the fact that the crystalline region in PLA samples hindered the diffusion and escape of CO_2.

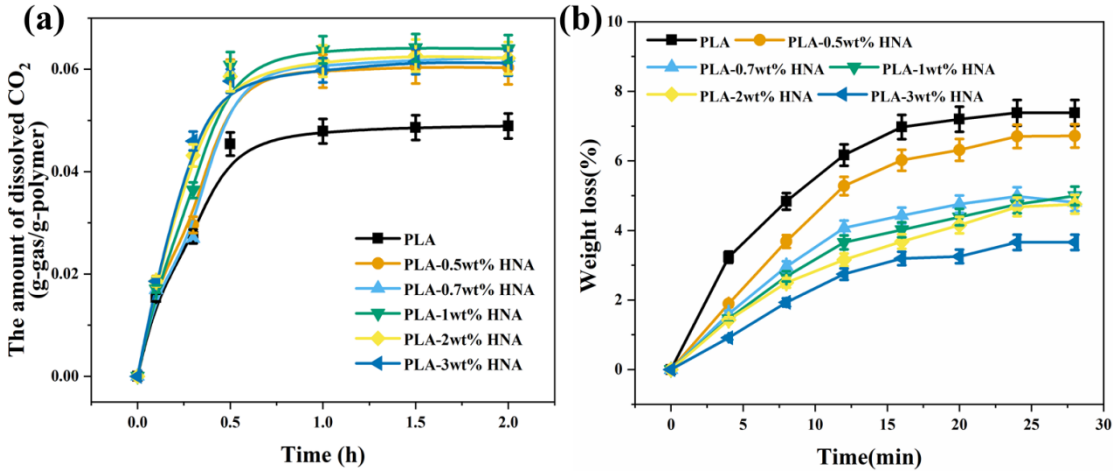

Figure 7. The amount of CO_2 dissolved in PLA and PLA-HNA samples (a), Desorption curves of saturated neat PLA and PLA-HNA samples (b)

3.3 Formation of Enhanced Microcellular Structure

The cell morphologies of PLA foams with different content of HNA were shown in Figure 8. For neat PLA foam, it presented polygon cellular structure with large cell size and uneven cell size distribution. In contrast, by incorporation of HNA, elliptical cells with much smaller cell size can be observed.

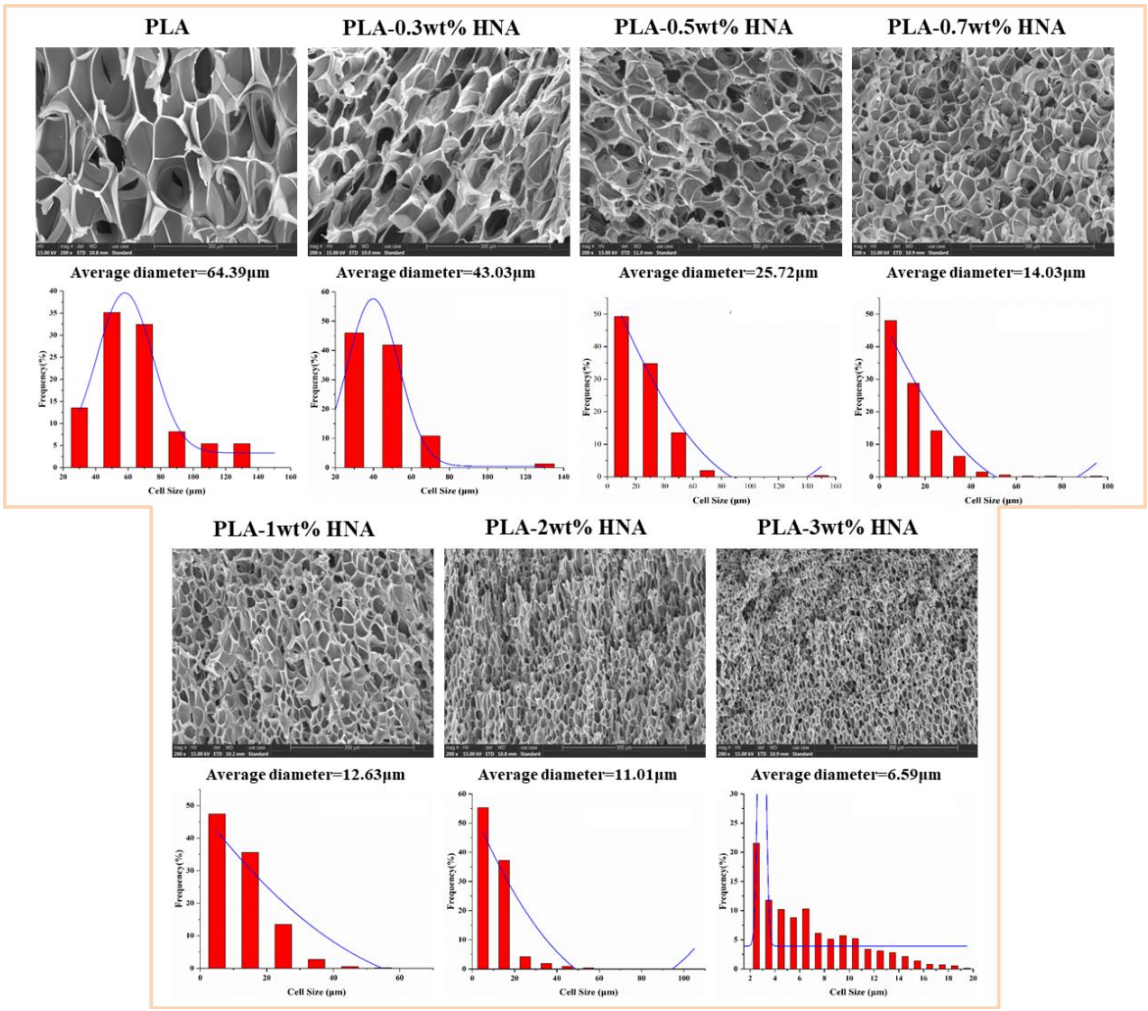

Figure 8. SEM images and cell size distribution of PLA-HNA foams with different HNA content

The structure of the cell wall of neat PLA and PLA-HNA foams was observed in detail as shown in Figure 9. It can be seen that, for neat PLA foam, very smooth cell walls can be observed. In contrast, for the PLA-HNA foam, lots of fibrillar structure appeared and entangled with each other. Such entangled fibrillar structure with high aspect ratio and high crystallinity can acted as a “pillar” structure to improve the ability of cell wall to resist deformation, and thus delay the damage and collapse of the cell.

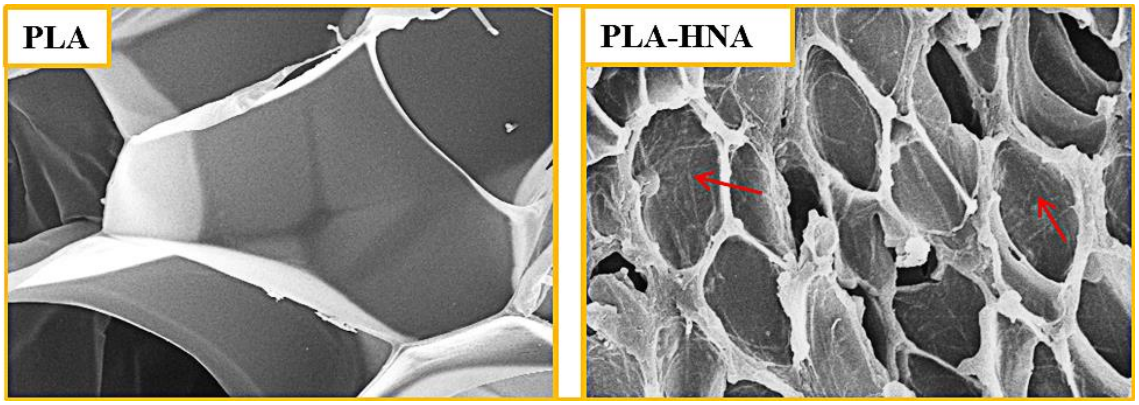

Figure 9. Morphology of the cell wall of neat PLA and PLA-HNA foams

Figure 10 summarized the average cell density, cell size, apparent density and expansion ratio of the PLA-HNA foams. With the increase of HNA content, the cell density and apparent density of PLA foam increased remarkably, while the average cell size and expansion ratio decreased. By incorporation of 3wt% HNA, the cell density of PLA foam reached 4.44×10^{9} cells/cm^{3}, which was three orders of magnitude higher than that of neat PLA foam, and the average cell size decreased to 6.59μm, reaching the level of microcellular foam.

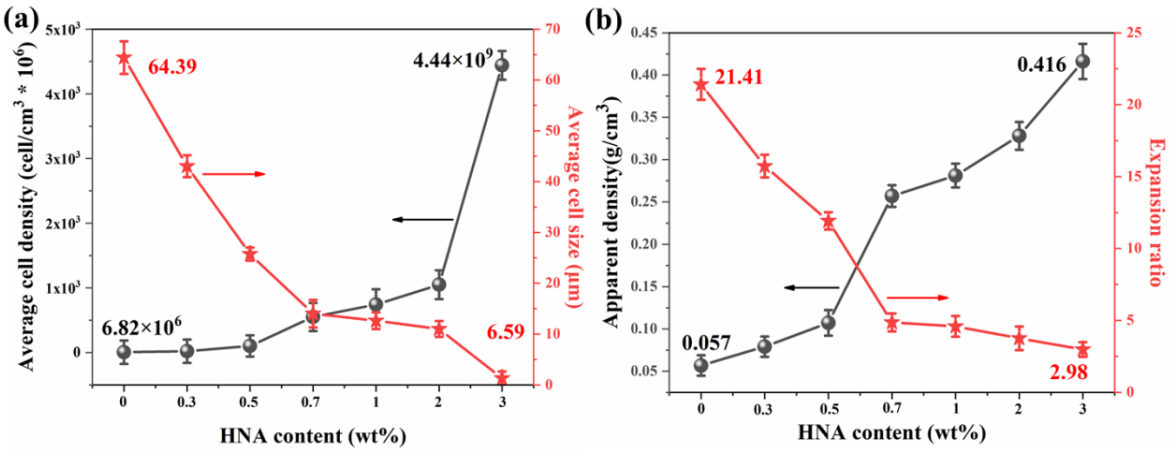

Figure 10. Average cell density and average cell size (a); apparent density and expansion ratio (b) of PLA-HNA foams with different HNA content

3.4 Mechanical Properties and Formation Mechanism of Enhanced Microcellular Structure for PLA-HNA Foam

The compressive strength and compressive modulus of PLA-HNA foams were illustrated in Figure 11. With increasing HNA content, both compressive strength and compressive modulus of PLA foam increased remarkably, exhibiting excellent

compression resistance.

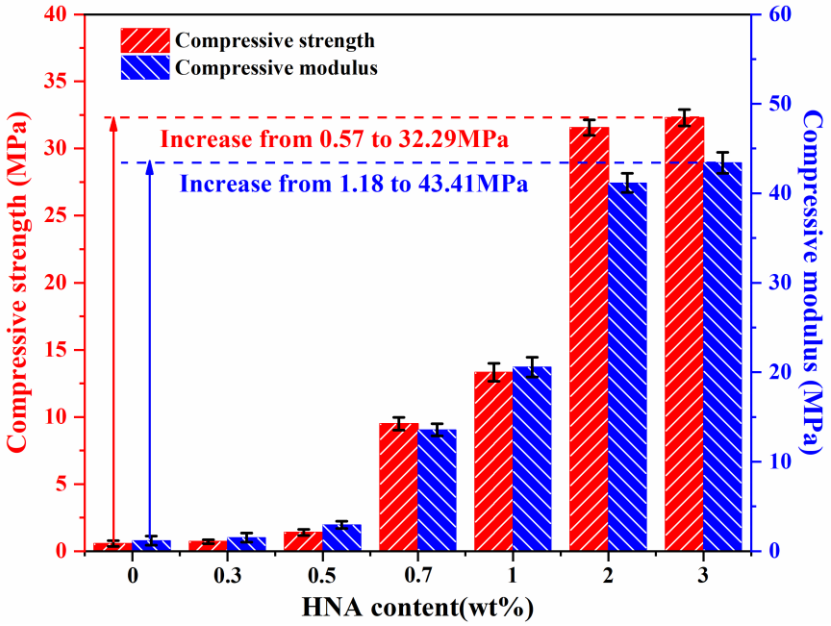

Figure 11. Compressive properties of PLA-HNA foams with different HNA content

In summary, the formation mechanism of enhanced microcellular structure for PLA-HNA foam was proposed, as illustrated in Figure 12. For neat PLA, due to the poor crystallization ability, sporadic and small spherulites formed in the sample. Meanwhile, the low viscoelasticity resulted in the occurrence of cell coalescence and cell-wall rupture, and thus foams with low cell density and large cell size were obtained. For PLA-HNA, incorporation of HNA not only increased the crystallinity of PLA obviously, but also promoted the formation of enhanced shish-kebab crystalline structure, which was beneficial for improving the viscoelasticity of PLA and reducing the cell coalescence of the foam. Moreover, the abundant interface between crystalline and amorphous regions provided lots of sorption sites for CO_2, while the crystalline structure could hinder the escape of CO_2 from the matrix, leading to an increase in the amount of dissolved CO_2 and a decrease in CO_2 desorption ratio for PLA-HNA samples. In addition, the crystal-amorphous region interface can also provide lots of heterogeneous nucleating sites for cell nucleation. Therefore, abundant gas can be wrapped efficiently in the cells and dense micropores (high apparent

density) were obtained for PLA-HNA sample. The dense cell structure together with the enhanced fibrillar structure on the cell wall contributed to the significantly improved compressive strength and modulus for PLA-HNA foams.

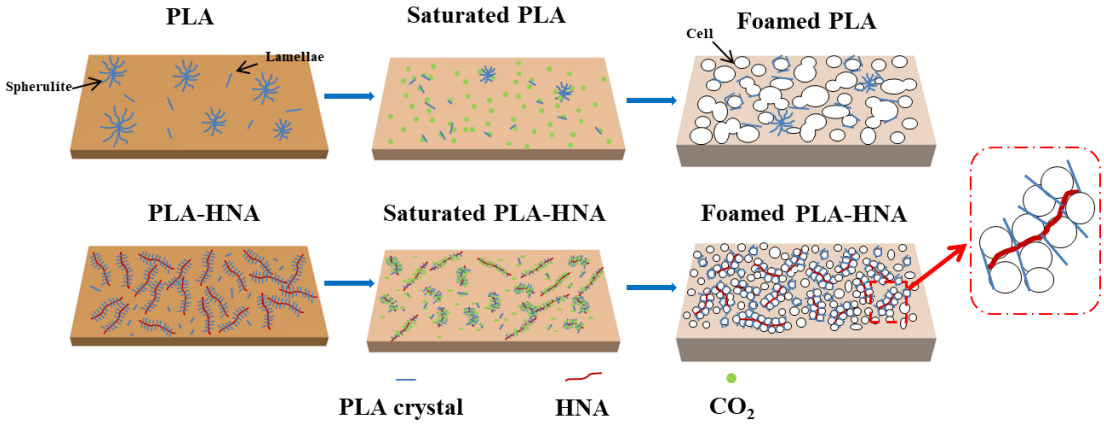

Figure 12. Schematic illustration of the foaming process of neat PLA and PLA-HNA

4. Conclusions

HNA was incorporated into PLA to tailor the crystallization behavior and PLA-HNA foams with microcellular structure were prepared via supercritical CO_2 foaming. HNA can precipitate prior to the crystallization of PLA and self-assemble into fibrillar networks, inducing the crystallization of PLA on their surface, and thus "shish-kebab" structure formed. The crystallization temperature moved to lower temperature for PLA-HNA, and the crystallinity increased with increasing HNA content. Compared with neat PLA, the variation of the intensities of bands at 1758 cm^{-1} for PLA-2wt% HNA sample was larger, indicating that higher population of gt conformer formed. Addition of HNA not only significantly increased the amount of CO_2 dissolved in PLA, but also improved the viscoelasticity of PLA matrix significantly. Compared with the neat PLA foam, by introduction of HNA, the average cell diameter of PLA-HNA foam decreased dramatically, from 64.39μm to 6.59μm, and the cell density increased remarkably, from 6.82×10^{6} cells/cm^3 to 4.44×10^{9} cells/cm^3, reaching the microcellular level. Due to the formation of dense micropores and enhanced crystalline structures on the cell wall of the foam, PLA

foam was highly reinforced with significantly improved compressive strength and modulus.

Acknowledgements

This research was financially supported by National Natural Science Foundation of China (Grant No. 51773122) and State Key Laboratory of Polymer Materials Engineering (Grant No. sklpme2019-2-21).

References

[1] Bao, J.; Weng, G.; Zhao, L. Tensile and impact behavior of polystyrene microcellular foams with bi-modal cell morphology. *J Cell Plast* **2014**, 50, 381-393.

[2] Miller, D.; Kumar, V. Microcellular and nanocellular solid-state polyetherimide (PEI) foams using sub-critical carbon dioxide II. Tensile and impact properties. *Polymer* **2011**, 52, 2910-2919.

[3] Kohlhoff, D.; Ohshima, M. Open cell microcellular foams of polylactic acid (PLA) ‐ based blends with semi ‐ interpenetrating polymer networks. *Macromol Mater Eng* **2011**, 296, 770-777.

[4] Ma, Z.; Zhang, G.; Yang, Q. Fabrication of microcellular polycarbonate foams with unimodal or bimodal cell-size distributions using supercritical carbon dioxide as a blowing agent. *J Cell Plast* **2014**, 50, 55-79.

[5] Pinto, J.; Reglero-Ruiz, J.; Dumon, M.; M, Rodriguez-Perez. Temperature influence and CO2 transport in foaming processes of poly (methyl methacrylate)–block copolymer nanocellular and microcellular foams. *J Supercrit Fluid* **2014**, 94, 198-205.

[6] Khorasani, M.; Ghaffarian, S.; Babaie, A. Foaming behavior and cellular structure of microcellular HDPE nanocomposites prepared by a high temperature process. *J Cell Plast* **2010**, 46, 173-190.

[7] Keramati, M.; Ghasemi, I.; Karrabi, M.; Azizi, H. Microcellular foaming of PP/EPDM/organoclay nanocomposites: the effect of the distribution of nanoclay on foam morphology. *Polym J* **2012**, 44, 433.

[8] Gong, P.; Buahom, P.; Tran, M.; Saniei, M.; Park, C.; Potschke, P. Heat transfer in microcellular polystyrene/multi-walled carbon nanotube nanocomposite foams. *Carbon* **2015**, 93, 819-829.

[9] Gedler, G.; Antunes, M.; Realinho, V.; Velasco, J. Thermal stability of polycarbonate-graphene nanocomposite foams. *Polym Degrad Stabil* **2012**, 97, 1297-1304.

[10] Wang, G.; Zhao, G.; Dong, G.; Mu, Y.; Park, C.; Wang, G. Lightweight, super-elastic, and thermal-sound insulation bio-based PEBA foams fabricated by high-pressure foam injection molding with mold-opening. *Eur Polym J* **2018**, 103, 68-79.

[11] Reignier, J.; Gendron, R. Mechanical anisotropy of PS/CO2 microcellular foam sheet

prepared by foaming extrusion. *J Cell Plast* **2018**, 54, 87-101.

[12] Wang, M.; Xie, L.; Qian, B.; Ma, Y.; Zhou, N. Extrusion foaming behavior of a polypropylene/nanoclay microcellular foam. *J Appl Polym Sci* **2016**, 133.

[13] Zhi, X.; Liu, J.; Zhang, H.; Hong, S.; Yu, Z. Simultaneous enhancements in electrical conductivity and toughness of selectively foamed polycarbonate/polystyrene/carbon nanotube microcellular foams. *Compos Part B-Eng* **2018**, 143, 161-167.

[14] Li, R.; Li, J.; Zhao, X.; Ye, L.; Coates, P.; Caton-Rose, F. Controlled in Vitro Degradation Behavior of Highly Oriented Long-chain-branched Poly (lactic acid) Produced by Solid-phase Die Drawing. *J Biomed Mater Res A* **2019**, 107, 1522-1531.

[15] Li, Z.; Zhao, X.; Ye, L.; Coates, P.; Caton-Rose, F. Structure and blood compatibility of highly oriented poly (l-lactic acid) chain extended by ethylene glycol diglycidyl ether. *Polymer* **2015**, 56, 523-534.

[16] Yuan, X.; Mak, A.; Kwok, K.; Yung, B.; Yao, K. Characterization of poly (L‐lactic acid) fibers produced by melt spinning. *J Appl Polym Sci* **2001**, 81, 251-260.

[17] Zhao, X.; Ye, L.; Coates, P.; Caton-Rose, F. Structure and blood compatibility of highly oriented poly (lactic acid)/thermoplastic polyurethane blends produced by solid hot stretching. *Polym Advan Technol* **2013**, 24, 853-860.

[18] Corre, Y.; Maazouz, A.; Duchet, J.; Reignier, J. Batch foaming of chain extended PLA with supercritical CO2: Influence of the rheological properties and the process parameters on the cellular structure. *J Supercrit Fluid* **2011**, 58, 177-188.

[19] Mihai, M.; Huneault, M.; Favis, B. Rheology and extrusion foaming of chain‐branched poly (lactic acid). *Polym Eng Sci* **2010**, 50, 629-642.

[20] Nofar, M.; Tabatabaei, A.; Sojoudiasli, H.; Park, C.; Carreau, P.; Heuzey, M.; Kamal, M. Mechanical and bead foaming behavior of PLA-PBAT and PLA-PBSA blends with different morphologies. *Eur Polym J* **2017**, 90, 231-244.

[21] Colton, J.; Suh, N. The nucleation of microcellular thermoplastic foam with additives: Part I: Theoretical considerations. *Polym Eng Sci* **1987**, 27, 485-492.

[22] Taki, K.; Kitano, D.; Ohshima, M. Effect of growing crystalline phase on bubble nucleation in poly (L-lactide)/CO_2 batch foaming. *Ind Eng Chem Res* **2011**, 50, 3247-3252.

[23] Zhang, Y.; Liu, D.; Dai, S.; Lu, H. Surfactant-Free Microemulsion Based on CO2-Induced

Ionic Liquids. *J Phys Chem B* **2019**, 123, 9024-9030.

[24] Li, B.; Zhao, G.; Wang, G.; Zhang, L.; Gong, J. Fabrication of high-expansion microcellular PLA foams based on pre-isothermal cold crystallization and supercritical CO_2 foaming. *Polym Degrad Stabil* **2018**, 156, 75-88.

[25] Tiwary, P.; Park, C B.; Kontopoulou, M. Transition from microcellular to nanocellular PLA foams by controlling viscosity, branching and crystallization. *Eur Polym J* **2017**, 91, 283-296.

[26] Nieddu, E.; Mazzucco, L.; Gentile, P.; Benko, T.; Balbo, V.; Mandrile, R.; Ciardelli, G. Preparation and biodegradation of clay composites of PLA. *React Funct Polym* **2009**, 69, 371-379.

[27] Wang, X.; Mi, J.; Zhou, H.; Wang, X. Transition from microcellular to nanocellular chain extended poly (lactic acid)/hydroxyl-functionalized graphene foams by supercritical CO_2. *J Mater Sci* **2019**, 54, 3863-3877.

[28] Geng, L.; Peng, X.; Jing, X.; Li, Leng.; Huang, A.; Xu, B.; Chen, B.; Mi, Hao. Investigation of poly (L-lactic acid)/graphene oxide composites crystallization and nanopore foaming behaviors via supercritical carbon dioxide low temperature foaming. *J Mater Res* **2016**, 31, 348-359.

[29] Culhacioglu, Y.; Hasirci, N.; Dilek, C. Highly Crystalline Poly (l-lactic acid) Porous Films Prepared with CO2-philic, Hybrid, Liquid Cell Nucleators. *Ind Eng Chem Res* **2019**, 58, 22541-22550.

[30] Nakajima, H.; Takahashi, M.; Kimura, Y. Induced Crystallization of PLLA in the Presence of 1, 3, 5‐Benzenetricarboxylamide Derivatives as Nucleators: Preparation of Haze‐Free Crystalline PLLA Materials. *Macromol Mater Eng* **2010**, 295, 460-468.

[31] Nofar, M.; Zhu, W.; Park, C. B.; Randall, J. Crystallization Kinetics of Linear and Long-Chain-Branched Polylactide. *Ind. Eng.Chem. Res* **2011**, 50, 13789−13798.

[32] Li, C.; Xiang, M.; Ye, L. Intercalation structure and highly enhancing tribological performance of monomer casting nylon-6/graphene nano-composites. *Compos Part A-Appl S* **2017**, 95, 274-285.

[33] Xing, Q.; Li, R.; Dong, X.; Luo, F.; Kuang, X.; Wang, D.; Zhang, L. Enhanced Crystallization Rate of Poly (l‐lactide) Mediated by a Hydrazide Compound: Nucleating Mechanism Study. *Macromol Chem Phys* **2015**, 216, 1134-1145.

[34] Lorenzo, D. Calorimetric analysis of the multiple melting behavior of poly (L‐lactic acid). *J Appl Polym Sci* **2006**, 100, 3145-3151.

Figure Captions

Table Captions

Graphical Abstract